J Biosci (2019) 44:93
DOI: 10.1007/s12038-019-9900-8

PET imaging study of brown adipose tissue (BAT) activity in mice devoid of receptor for advanced glycation end products (RAGE)

YU-SHIN DING[1,2]*, NOEEN MALIK[1], SEBASTIAN MENDOZA[1], DANIEL TUCHMAN[1], CARMEN HURTADO DEL POZO[3], RAQUEL LOPEZ DIEZ[3] and ANN-MARIE SCHMIDT[3]

[1]*Department of Radiology, New York University School of Medicine, New York, USA*

[2]*Department of Psychiatry, New York University School of Medicine, New York, USA*

[3]*Diabetes Research Program, Division of Endocrinology, Department of Medicine, New York University School of Medicine, New York, USA*

**Corresponding author (Email, yu-shin.ding@nyumc.org)*

MS received 29 October 2018; accepted 29 April 2019; published online 6 August 2019

Brown adipose tissue (BAT) is responsible for adaptive thermogenesis. We previously showed that genetic deficiency of receptor for advanced glycation end products (RAGE) prevented the effects of high-fat diet (HFD). This study was to compare BAT activity in RAGE knock out (*Ager*$^{-/-}$, RKO) and wild-type (WT) mice after treated with HFD or LFD. [^{18}F]FDG PET-CT imaging under identical cold-stimulated conditions and mean standard uptake values (SUV_{mean}), ratio of SUV_{iBAT}/SUV_{muscle} (SUVR, muscle as the reference region) and %ID/g were used for BAT quantification. The results showed that [^{18}F]FDG uptake (e.g., SUVR) in WT-HFD mice was significantly reduced (three-fold) as compared to that in WT-LFD (1.40 ± 0.07 and 4.03 ± 0.38; $P = 0.004$). In contrast, BAT activity in RKO mice was not significantly affected by HFD, with $SUVR_{RKO\text{-}LFD}$: 2.14 ± 0.10 and $SUVR_{RKO\text{-}LFD}$: 1.52 ± 0.13 ($P = 0.3$). The uptake in WT-LFD was almost double of that in RKO-LFD ($P = 0.004$); however, there was no significant difference between RKO-HFD and WT-HFD mice ($P = 0.3$). These results, corroborating our previous findings on the measurement of mRNA transcripts for *UCP1* in the BAT, suggest that RAGE may contribute to altered energy expenditure and provide a protective effect against HFD by *Ager* deletion (*Ager* $^{-/-}$).

Keywords. Brown adipose tissue; [^{18}F]FDG; high-fat diet; obesity; PET/CT; RAGE

Abbreviations: BAT, brown adipose tissue; UCP1, uncoupling protein 1; RAGE, receptor for advanced glycation end products; HFD, high-fat diet; LFD, low-fat diet; WT, wild type; RKO, RAGE knock out; *Ager* $^{-/-}$, *Ager* deletion; iBAT, interscapular BAT; SUV_{mean}, mean standard uptake values; SUVR, ratio of SUV_{iBAT}/SUV_{muscle}; ID/g, injected dose per gram; β_3-AR, β_3-adrenergic receptors; IRW, Inveon research workplace; DIO, diet-induced obesity

1. Introduction

In humans, adipocytes play a key role in the regulation of whole body energy homeostasis. To maintain such an energy balance, there are two major types of adipocytes: white adipose tissue (WAT, responsible for energy storage, such as in the form of lipids) and brown adipose tissue (BAT, dissipates and expends energy for non-shivering and adaptive thermogenesis) (Zhuang *et al.* 2001; Chavakis *et al.* 2004; Cypess and Kahn 2010; Virtanena and Nuutila 2010; Nedergaard and Cannon 2013; Bartelt and Heeren 2014; Cao *et al.* 2014; Lau *et al.* 2015; Thoonen *et al.* 2016). In addition to heat balance, BAT not only acts as an endocrine organ by signaling multiple tissues after adipokine secretions (Cairo *et al.* 2016), but it also plays an important role in insulin resistance, hyperlipidemia, obesity and cancers such as breast and prostate cancers (Ishiguro *et al.* 2005; Cao *et al.* 2014; Bao *et al.* 2015). BAT is located in high density in the supraclavicular region in humans (Nirengi *et al.* 2015, 2016) and the interscapular region in rodents ($iBAT_{mice} \approx 200$ mg; sampled after dissection) (Walden *et al.* 2012; de Jong *et al.* 2015). Histological studies have shown that BAT activity is functionally controlled by mitochondrial inner membrane uncoupling protein 1 (UCP-1) triggered by β_3-adrenergic receptors (β_3-AR), which is activated by norepinephrine present in sympathetic nerves. Subsequently, the high expression of *UCP1* leads to mobilization of triglycerides after lipolysis from WAT to BAT; thus, heat is produced after uncoupling the electron transport chain (aerobic respiration) from oxidative phosphorylation (Zhuang *et al.* 2001;

Chavakis *et al.* 2004; Cypess and Kahn 2010; Virtanena and Nuutila 2010; Nedergaard and Cannon 2013; Bartelt and Heeren 2014; Cao *et al.* 2014; Lau *et al.* 2015; Thoonen *et al.* 2016). Thence, the activated BAT can clear 75% glucose and 50% triglycerides from blood after burning of triglycerides powered by glucose (Gifford *et al.* 2016).

There are several factors that affect BAT metabolism, such as gender, age, cold exposure (Mirbolooki *et al.* 2011; Lim *et al.* 2012; Hwang *et al.* 2015; Ding 2016), anesthesia (Tatsumi *et al.* 2004), intake of the β_3-AR inhibitor (e.g., propranolol) (Tatsumi *et al.* 2004), body-mass index, fasting and stimulation of pancreatic insulin (Zhuang *et al.* 2001). In addition to these, another essential contributor to the activity of BAT is receptor for advanced glycation end products (RAGE). RAGE is a multi-ligand receptor comprising three-main domains: one V-type (where ligand binds), two C-types and one cytosolic tail, responsible for intracellular signaling during RAGE-activation (Chavakis *et al.* 2004). This receptor shows low expression in normal tissues but is upregulated and highly expressed in RAGE-expressing tissues such as immune cells, adipose tissues and liver (Song *et al.* 2014). During the intake of a high-fat diet (HFD), the production and the increased accumulation of advanced glycated end products in metabolic tissues lead to the inflammations that ultimately result in complications such as diabetes mellitus, obesity, adiposity, reduced thermogenesis, low-metabolic rate and neurodegenerative and cardiovascular diseases (Chavakis *et al.* 2004; Song *et al.* 2014).

It is known that glucose functions as a fuel in both adaptive and non-shivering thermogenesis by BAT (Hull and Segall 1965; Himms-Hagen 1990); thus, [^{18}F]FDG, a glucose analogue, represents a potential tracer to study BAT activity. We and others have previously performed successful preclinical and clinical studies using [^{18}F]FDG as a radiotracer for BAT quantification with positron emission tomography (PET) (Hull and Segall 1965; Lin *et al.* 2012; Wang *et al.* 2012; Azhdarinia *et al.* 2013; Borga *et al.* 2014). The results revealed that, in both humans and rodents, [^{18}F]FDG could quantitate BAT reliably under mild cold stimulations (Hull and Segall 1965; Lin *et al.* 2012; Wang *et al.* 2012; Hwang *et al.* 2015; Ding 2016).

Our previous study demonstrated that genetic deficiency of RAGE prevented the effects of HFD on adipose tissue inflammation, obesity and insulin resistance (Song *et al.* 2014). The aim of the present study was to directly compare, via *in vivo* PET imaging, the BAT activity in RAGE null and wild-type (WT) mice in response to different diet conditions; i.e., to characterize the uptake of [^{18}F]FDG in the BAT of RAGE-deficient mice (RKO, RAGE knock out, *Ager* $^{-/-}$) *vs* WT mice, under HFD and low-fat diet (LFD) conditions.

2. Materials and methods

2.1 *Preparation of animals*

Homozygous RAGE null mice (C57BL/6 *Ager*$^{-/-}$ mice backcrossed > 20 generations into C57BL/6J) and their littermate RAGE-expressing controls (C57BL/6J, WT) (The Jackson Laboratory, Bar Harbor, ME) were used. All mice studied were male, had free access to water, and were subjected to 12 h light/dark cycles. At 6–8 weeks of age, mice were fed a HFD with 60% of calories from lard (D12492; Research Diets, Inc., New Brunswick, NJ) or a LFD with 13% of calories from fat (5053 PicoLab Rodent Diet 20; LabDiet, Brentwood, MO) for 2 months before imaging. All animal procedures were approved by the New York University Medical School Institutional Animal Care and Use Committees and performed in accordance with the National Institutes of Health Animal Care Guidelines.

2.2 *PET/computed tomography(CT) imaging*

All animals were fasting for at least 4 h before scans. Before imaging, mice were anesthetized with isoflurane (2–3%) and cannulated in tail vein using home-made cannulas that were prepared using 30 G needles (Exel International Hypodermic) and 2″ tubing (Intramedic^{TM} PE Tubing, 0.011″ ID). Mice were then taped in a flat, prone position with arms at sides in a home-made mouse holder.

A high-resolution micro PET/CT system (Siemens, Inveon) was used for imaging. The mouse was wrapped with a cold-pack (108 g of cooling gel, 4°C) and placed under isoflurane anesthesia on the bed of the scanner for 30 min before injection (and continuously under cold stimulation during the entire scan). [^{18}F]FDG (300–400 μCi in 200 μL of saline) was injected, which was chased with another 200 μL of saline. All intravenous tail-vein injections *via* cannulas were performed right before the initiation of the dynamic PET acquisition. After the PET dynamic acquisition (60 min), CT acquisition (6 min) was carried out for attenuation correction and co-registration. The PET histogram was then created followed by PET reconstruction using the OSEM2D algorithm.

2.3 *Data analysis*

PET image data were analyzed using an Inveon research workplace (IRW, Siemens). The investigators responsible for data analysis were blinded to which animals represent control and experiment groups. The values of [^{18}F]FDG uptake using different parameters such as standard uptake values (SUV) or %injected dose per gram (%ID/g) for uptake in interscapular BAT (iBAT) (regions of interest, ROIs) were determined.

For PET datasets, SUV by body weight was used for the quantification based on the time-activity data (see the Results section).

$$\mathrm{SUV} = \frac{\text{average activity in ROI (Bql/mL)}}{\text{injected dose (Bql)}} * \text{subject weight (g)}$$

The quantity of %ID/g is a measure of the proportion of the injected dose within the area that is selected. For example, if 10 MBq of activity is injected into the subject, and a particular ROI had an average intensity value of 1 MBq/mL, the %ID/g value for that ROI would be 10%.

To eliminate inter-subject variations, a reference region (muscle) was chosen and ratios of SUV_{iBAT} to SUV_{muscle} (SUVR) were calculated. ROIs were drawn using the same volume for both iBAT and muscle for each study animal. The time–activity curves of %ID/g and SUV for each ROI from each mouse were then obtained from the IRW.

2.4 *Statistical analysis*

All parameters for each group were averaged and expressed as mean ± SEM. Statistical analyses were performed using SPSS (IBM SPSS version 20). Normality tests were performed on each measurement. Between-group comparisons were performed using unpaired *t*-tests (assumes normality for differences), as well as non-parametric Mann–Whitney *U* tests (not assumes normality for differences) (p value of <0.05 is considered statistically significant). One-way ANOVA (comparing three or more groups) or two-way ANOVA (ordinary two-way ANOVA, not repeated measures) was also performed.

3. Results

Time–activity curves (%ID/g, SUV and SUVR) for four sub-groups of mice (RKO-LFD, RKO-HFD, WT-LFD and WT-HFD), plotted along with the corresponding SEM values, are shown in figure 1. All measurements (%ID/g, SUV and SUVR) peaked within the first few time frames (0–5 min), decreased gradually from 10 to 20 min, and then reached a plateau after 30 min (figure 1a–c (display only the late time frames when the values reached a plateau)). Each measurement (%ID/g, SUV and SUVR) was then quantitated in three-different ways based on the time–activity data: (a) as a direct average from the entire 60 min (DtAvg); (b) as a direct average from frames 30–60 min (DtAvg_f30–60, when the values reached a plateau; i.e., pseudo-equilibrium state); or (c) as weighted averages of the entire dynamic study (WtAvg, i.e., each measurement from a specific time frame was multiplied by the duration of the time frame. Summing all these measurements, followed by dividing by the entire duration of all frames, afforded the weighted averages). These results are tabulated in table 1 ($n = 6$ for each group).

Using unpaired *t*-tests (assumes normality for differences) or non-parametric Mann–Whitney *U* tests (does not assume normality for differences), or ANOVA (one-way or two-way), the outcome for group comparisons were similar.

The trend for %ID/g observed among all four sub-groups was, for example, RKO-LFD (2.42 ± 0.26) ≥ RKO-HFD (2.21 ± 0.18) ≥ WT-HFD (1.86 ± 0.34) ≥ and WT-LFD (1.64 ± 0.30) (table 1, ID-g_WtAvg). There was no significant difference in %ID/g in comparison with any two groups (WT-HFD *vs.* WT-LFD: $P = 0.5$; RKO-LFD *vs.* RKO-HFD: $P = 0.5$; WT-LFD *vs.* RKO-LFD: $P = 0.5$; RKO-HFD *vs.* WT-HFD: $P = 0.3$) (figure 2a).

In SUV comparison within the same strain groups, HFD made a significant impact on WT mice with a significantly lower uptake of [^{18}F]FDG in iBAT of WT-HFD (SUV: 0.48 ± 0.03) than that of WT-LFD (SUV: 1.59 ± 0.16) ($P = 0.004$). In contrast, HFD had no significant impact on the [^{18}F]FDG uptake in iBAT of RKO mice, with SUV values of 0.62 ± 0.05 and 0.92 ± 0.06 for RKO-HFD and RKO-LFD, respectively ($P = 0.3$) (table 1, SUV_WtAvg_-BAT, and figure 2b). A similar trend was also obtained for the SUV_DtAvg_f30-60_BAT measurement (table 1).

To eliminate inter-subject variations, a reference region (muscle) was chosen and SUVR were calculated. We found that SUVR_DtAvg_f30_60 and SUVR_WtAvg provided similar statistical outcomes with similar significance levels (p values) for most group comparisons.

As shown in table 1, the uptake of [^{18}F]FDG in muscle was lower than that in iBAT, and close to constant for all four groups (≈ 0.4), suggesting that muscle is a suitable reference region. In intra-group comparison, the SUVR values derived from SUVR_WtAvg showed an almost three-fold higher uptake in WT-LFD (4.03 ± 0.38) than in WT-HFD (1.40 ± 0.07) ($P = 0.004$), suggesting high-adipose tissue inflammation in the presence of RAGE in WT. In contrast, the RKO-HFD had only slightly reduced uptake of [^{18}F]FDG in iBAT than RKO-LFD ($SUVR_{RKO\text{-}LFD}$: 2.14 ± 0.10, $SUVR_{RKO\text{-}HFD}$: 1.52 ± 0.13), which did not reach a significant difference ($P = 0.3$) (table 1, SUVR_WtAvg) (figure 2c). In inter-group comparison, under LFD conditions, the uptake of [^{18}F]FDG in iBAT of WT-LFD control mice ($SUVR_{WT\text{-}LFD}$: 4.03 ± 0.38) was almost double than that in RKO-LFD ($SUVR_{RKO\text{-}LFD}$: 2.14 ± 0.10) ($P = 0.004$), whereas under HFD conditions, the uptake of [^{18}F]FDG in iBAT is similar for both groups ($SUVR_{RKO\text{-}HFD}$: 1.52 ± 0.13, $SUVR_{WT\text{-}HFD}$: 1.40 ± 0.07) ($P = 0.3$) (table 1) (figure 2c). A similar trend was observed when comparing the SUVR values derived from SUVR_DtAvg_f30-60 min (average from frames 30–60 min) (table 1, SUVR_DtAvg_f30-60 min) where the SUVR values reached the steady state (see figure 1c, time–activity curves of SUVR). PET/CT images for the [^{18}F]FDG uptake in iBAT of four sub-groups of mice (RKO-LFD, RKO-HFD, WT-LFD and WT-HFD) reflected these quantitative data and were consistent with these findings. A set of representative images are presented in figure 3a–d.

4. Discussion

In our previous work (Song *et al.* 2014), we showed that *Ager* genotype had no effect on weight gain under a LFD (i.e., similar body weight between RKO-LFD and WT-LFD

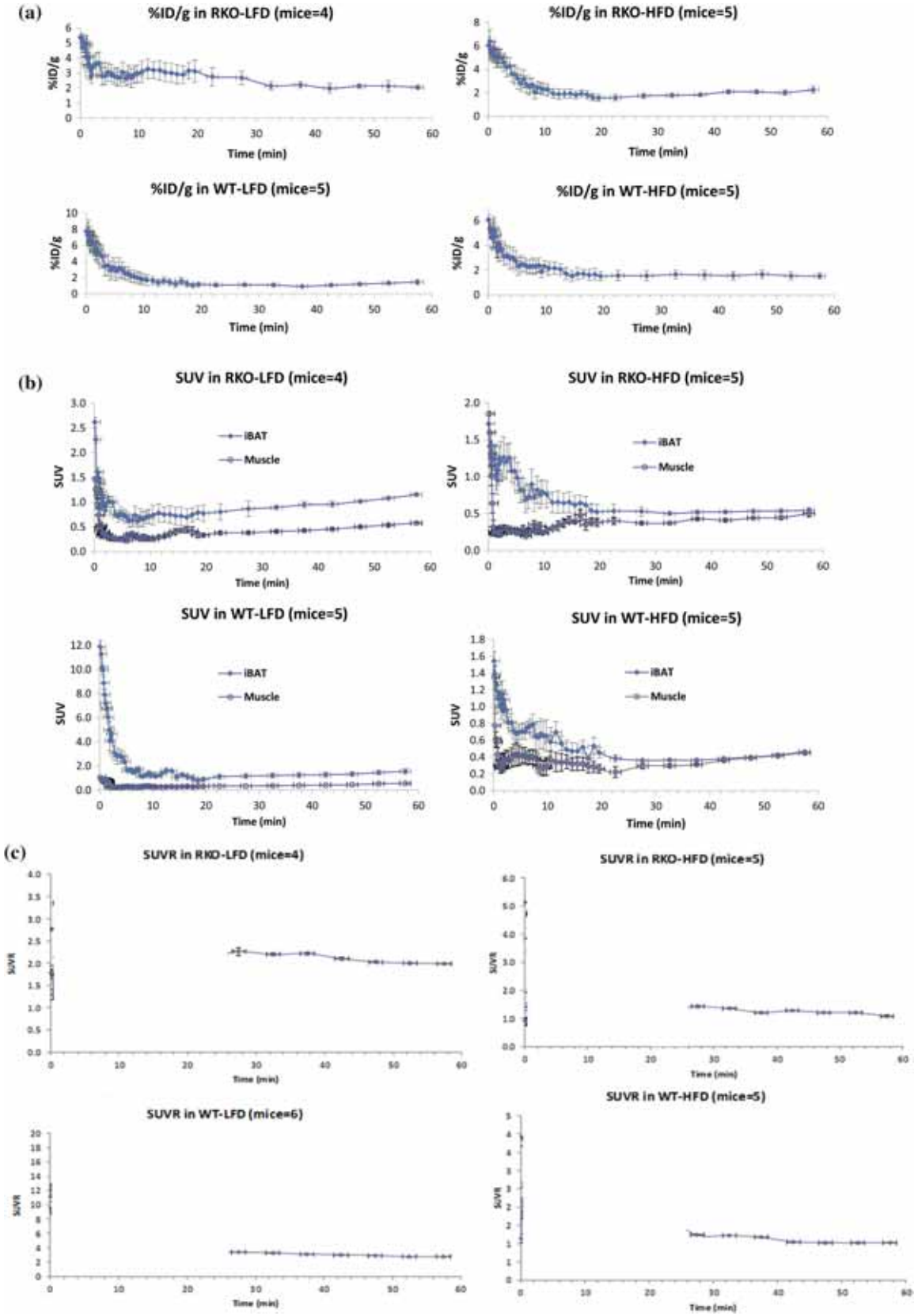

Figure 1. Time–activity curves for four sub-groups of mice: (**a**) % ID/g in iBAT, (**b**) SUV_{iBAT} and SUV_{muscle} and (**c**) SUVR (SUV_{iBAT}/SUV_{muscle}) (display only the late time frames when the values reached a plateau).

Table 1. Quantitative uptake values (%ID/g, SUV, or SUVR) in four sub-groups of two strains of mice (WT and RKO) under HFD or LFD conditions

	RKO-LFD	RKO-HFD	WT-LFD	WT-HFD
ID-g_DtAvg	3.23 ± 0.41	3.29 ± 0.39	3.23 ± 0.70	2.81 ± 0.45
ID-g_DtAvg_f30-60	2.12 ± 0.03	2.01 ± 0.07	1.20 ± 0.08	1.59 ± 0.03
ID-g_WtAvg	2.42 ± 0.26	2.21 ± 0.0.18	1.64 ± 0.30	1.86 ± 0.34
SUV_DtAvg_BAT	0.95 ± 0.07	0.88 ± 0.11	3.28 ± 0.19	0.74 ± 0.05
SUV_DtAvg_f30-60_BAT	1.01 ± 0.04	0.53 ± 0.01	1.35 ± 0.06	0.4 ± 0.02
SUV_WtAvg_BAT	0.92 ± 0.06	0.62 ± 0.05	1.59 ± 0.16	0.48 ± 0.03
SUV_DtAvg_MUS	0.44 ± 0.02	0.43 ± 0.02	0.44 ± 0.01	0.39 ± 0.04
SUV_DtAvg_f30-60_MUS	0.48 ± 0.03	0.43 ± 0.02	0.45 ± 0.03	0.37 ± 0.02
SUV_WtAvg_MUS	0.43 ± 0.01	0.41 ± 0.01	0.40 ± 0.01	0.35 ± 0.02
SUVR_DtAvg	2.18 ± 0.08	2.09 ± 0.28	7.60 ± 0.49	1.99 ± 0.16
SUVR_DtAvg_f30-60	2.09 ± 0.04	1.22 ± 0.04	2.99 ± 0.09	1.09 ± 0.07
SUVR_WtAvg	2.14 ± 0.10	1.52 ± 0.13	4.03 ± 0.38	1.40 ± 0.07

groups). In contrast, RAGE-deficient mice were protected from the weight gain experienced by WT mice when fed with a HFD; i.e., there was considerable gain in weight over 6 weeks for WT-HFD mice, but not for RKO-HFD mice. These results suggest that RAGE may play a role in diet-induced obesity (DIO) through, in part, its ability to modulate energy expenditure.

To test this hypothesis, we conducted a PET imaging study on BAT, a molecular target that is responsible for adaptive thermogenesis and energy expenditure. Although quantitative assessment and metabolic imaging of BAT using [^{18}F]FDG with PET have been previously reported (Tatsumi *et al.* 2004; Mirbolooki *et al.* 2011; Lim *et al.* 2012; Hwang *et al.* 2015; Ding 2016), the contribution of RAGE to DIO through the energy expenditure pathway has not been investigated with PET.

In order to study BAT activity/thermogenesis in mice, cold stimulation (4°C) was applied to all *in vivo* PET/CT scans since quantification of the [^{18}F]FDG uptake in iBAT is more reliable under mild cold conditions based on previous studies (Hull and Segall 1965; Tatsumi *et al.* 2004; Mirbolooki *et al.* 2011; Lim *et al.* 2012; Lin *et al.* 2012; Wang *et al.* 2012; Hwang *et al.* 2015; Ding 2016). The goal of this study was to investigate the impact of the RAGE receptor on BAT activity under different diet conditions. For proof-of-concept purposes, we compared the BAT activity under identical imaging conditions between two strains of C57/BL6 mice, WT (control mice with RAGE receptor) and RAGE knock out (*Ager* deletion, *Ager* $^{-/-}$, RKO), under different diet types: WT-LFD, WT-HFD, RKO-LFD and RKO-HFD.

In mice, BAT tissues are located in several regions, among which predominantly are iBAT ($\approx$200 mg), cervical BAT (cBAT $\approx$ 50 mg) and axillary BAT (aBAT $\approx$ 100 mg), as quantified via tissue sampling based on literature reports (Walden *et al.* 2012; de Jong *et al.* 2015). iBAT is the largest, deposited as two-symmetric lobes above the shoulder blades in rodents (Walden *et al.* 2012; de Jong *et al.* 2015), and is equally visualized as the BAT in the supraclavicular region in humans (Tatsumi *et al.* 2004; Mirbolooki *et al.* 2011; Lim *et al.* 2012; Hwang *et al.* 2015; Ding 2016). In our study, we observed predominantly uptake in iBAT in all mice (aBAT and cBAT have negligible or no uptake), which is consistent with the literature (Tatsumi *et al.* 2004; Mirbolooki *et al.* 2011; Lim *et al.* 2012; Hwang *et al.* 2015; Ding 2016).

The values of %ID/g, SUV and SUVR are shown in table 1 as a direct average of the entire scan (DtAvg), or a direct average from frames 30 to 60 min (DtAvg_f30-60), or weighted averages (WtAvg) of the entire dynamic study. As indicated in table 1 and figure 2a, RKO mice seem to have higher %ID/g values than those of WT mice, suggesting that RKO mice may have higher BAT mass; however, this difference did not reach significance.

Conventionally, SUV values of [^{18}F]FDG provide an index for BAT activation. In the time–activity curves shown in figure 1b, we noticed that there was a significantly higher uptake during the initial time frames in WT-LFD mice (all six mice) as compared to the other three groups of mice. That is, all six WT-LFD mice have an initial SUV at a range of 11–12, as compared to $\sim$2 for initial SUV for all mice in the other three groups. The rationale for this phenomenon is not clear. It may be due to a fast blood flow and fast tracer delivery that resulted in a higher initial SUV in WT-LFD mice. Potential interruption or hindrance in blood vessels could be, in part, the explanation for a slower blood flow in the genetically manipulated RKO mice or the WT-HFD mice.

For these reasons, SUVR with a reference region approach was used as the index for comparison to reduce the potential confounding effect due to the blood flow. Further, as for most PET imaging data analysis, the results are in general less variable when a reference region is used, e.g., distribution volume ratio (DVR; ratio of DV_{ROI} to DV_{ref}) or SUVR (SUV ratio; ratio of SUV_{ROI} to SUV_{ref}), as compared to the DV or SUV values derived from specific ROIs (Innis *et al.* 2007; Borga *et al.* 2014; Hwang *et al.* 2015; Ding

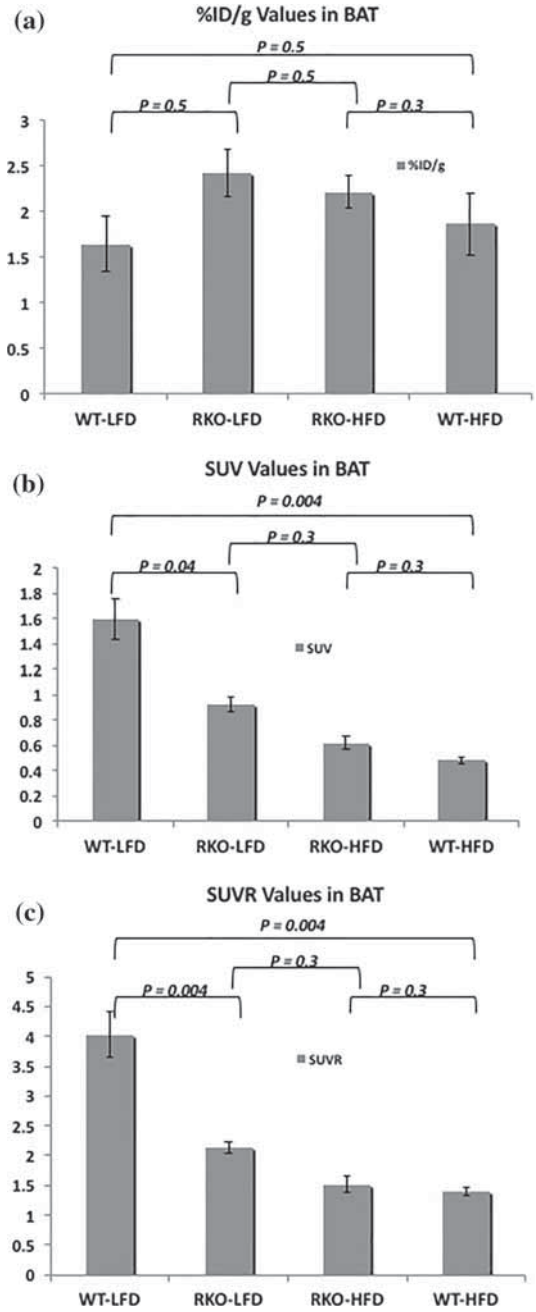

Figure 2. Bar graphs showing relative values (weighted average) of uptake in iBAT for: (**a**) %ID/g, (**b**) SUV_{iBAT} and (**c**) SUVR (SUV_{iBAT}/SUV_{muscle}) in four sub-groups of mice.

2016). Thus, the same voxel size of the muscle region as that for the iBAT region was drawn on each mouse image from all four groups and used as the reference region. The SUV values were determined and the SUVR were then calculated for each mouse, as shown in table 1. We found that SUVR_DtAvg_f30_60 and SUVR_WtAvg provided similar statistical outcomes.

It has been shown that *UCP1* in the brown-adipose tissue contributes a major role in energy expenditure (Fromme and Klingenspor 2011; Nedergaard and Cannon 2013; Kozak 2014) due to its high expression in BAT. No study has directly linked BAT activities with the *UCP1* mRNA and UCP1 protein. The results on changes in *UCP1* mRNA and UCP1 protein content in response to a HFD in mice and rats were varied (sometimes even opposite) when comparing different temperatures, strains, etc. (Fromme and Klingenspor 2011; Nedergaard and Cannon 2013). Nedergaard *et al.* also established an apparent lack of relationship between *UCP1* mRNA levels and UCP1 protein levels after a long period of acclimation to cold (30 days at 4°C). It was suggested that UCP1 protein levels are probably regulated pretranslationally; thus, the time delay obscures their change within the first few hours of cold exposure, as compared to the changes in *UCP1* mRNA levels.

We have previously measured mRNA transcripts for *UCP1* in the brown-adipose tissue of WT and RAGE null mice fed HFD *vs* LFD (Song *et al.* 2014). The mouse strains (WT and RAGE null), gender (all males), housing conditions, diet-treatment conditions (HFD or LFD) and the age during which the measurements were conducted, were identical between the previous and the present studies. In our present BAT imaging study design, animals were exposed to cold for less than 2 h and the study was conducted under the exact same cold stimulation conditions for all four groups. Although *UCP1* mRNA might be slightly increased with cold, this effect may not be an issue for our direct comparison among the four study groups, or for the correlation between the measurement of BAT activity (*via* PET in the present study) and the transcripts of *UCP1* mRNA in BAT (our previous study (Song *et al.* 2014)) for four study groups since the same experimental conditions were applied to four groups for both studies. Interestingly, excellent correlations were found between the transcripts of *UCP1* mRNA in BAT measured previously (figure 4) (Song *et al.* 2014) and the BAT activity measured with PET, especially when weighted averages SUVR for an entire dynamic study were used for correlations, as summarized in table 2.

(1) Our previous study showed that transcripts of *UCP1* mRNA were doubled in WT-LFD than in RKO (*Ager* $^{-/-}$)-LFD (Song *et al.* 2014), which was similar to what was observed in the current imaging study on BAT activity ($SUVR_{WT\text{-}LFD}$ (4.03) > $SUVR_{RKO\text{-}LFD}$ (2.1); $P = 0.004$).

(2) A significant difference was previously observed for transcripts of *UCP1* mRNA in WT between HFD and LFD mice. Similarly, the BAT activity in the present study was significantly reduced in WT-HFD as compared to WT-LFD as evidenced by the [^{18}F]FDG uptake ($P = 0.004$).

(3) In contrast, the difference in the *UCP1* mRNA transcripts between RKO-LFD and RKO-HFD mice did not reach significance. This was also observed in the present BAT imaging study ($SUVR_{RKO\text{-}HFD} \approx SUVR_{RKO\text{-}LFD}$; $P = 0.3$).

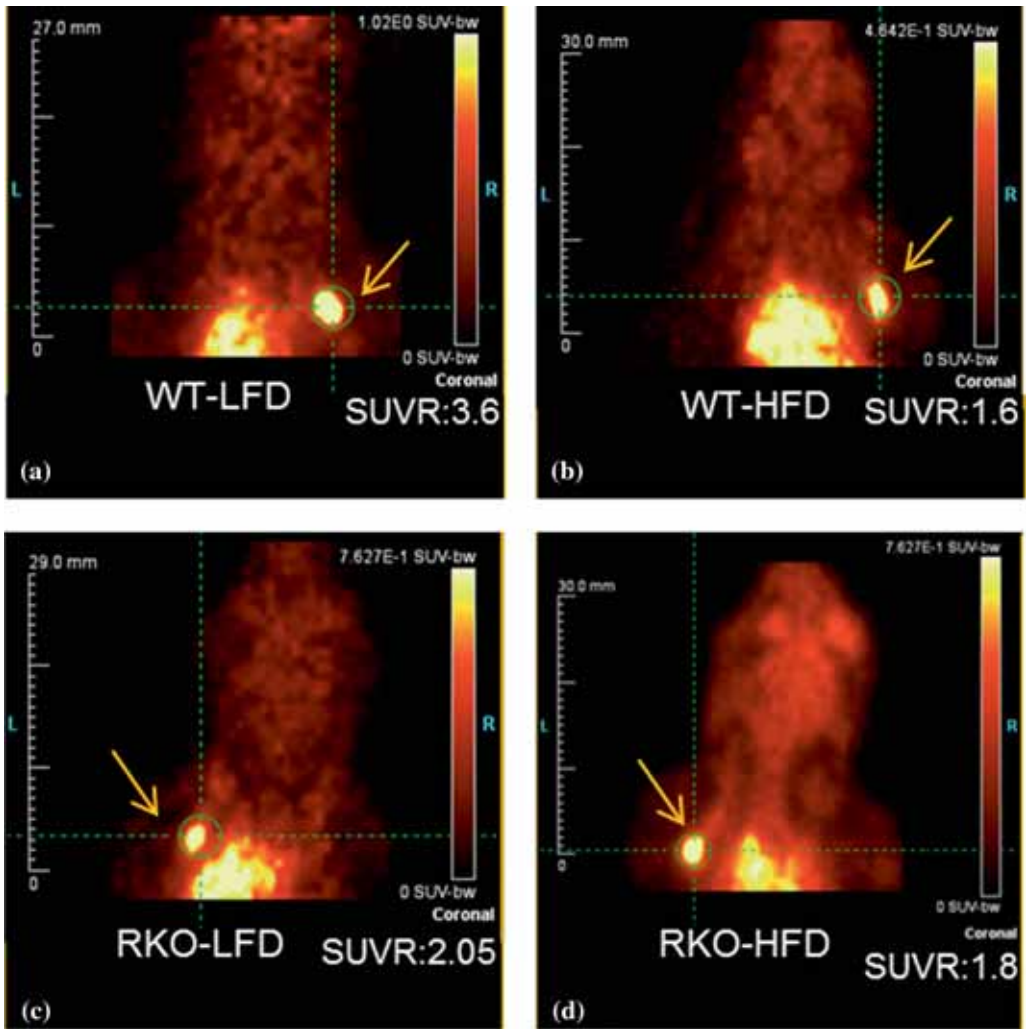

Figure 3. PET images (coronal sections) of four sub-groups of mice: (**a**) WT-LFD, (**b**) RKO-LFD, (**c**) WT-HFD and (**d**) RKO-HFD.

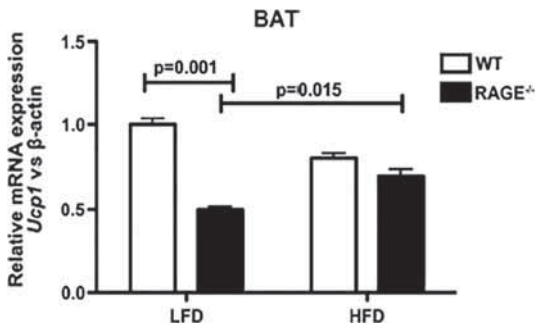

Figure 4. Effects of *Ager* genotype on BAT levels of *UCP1* mRNA transcripts. Wild-type or RAGE null mice were subjected to LFD or HFD for 2 months; at the end of that time, BAT was retrieved and subjected to a real-time polymerase chain reaction for quantification of *UCP1* mRNA transcripts. $N = 6$ mice/group. (Reproduced supplementary figure 6 from our previous study Song *et al.* 2014.)

(4) Further intergroup comparisons showed that in high-fat feeding, *UCP1* mRNA transcripts in BAT did not differ between WT-HFD and RAGE-HFD null mice. Consistent results were seen between the BAT activity of RKO-HFD and WT-HFD, which was not significantly different ($P = 0.3$).

5. Conclusion

In conclusion, in WT mice (in the presence of RAGE), HFD presented detrimental effects on energy expenditure by significantly reducing the BAT activity, which is evident by lower uptake of [^{18}F]FDG in WT-HFD than in WT-LFD ($P = 0.004$). This may be due to the adipose tissue inflammation caused by increased accumulation of AGEs. In contrast, in the case of RAGE deficiency, a HFD exhibited no significant effect on BAT thermogenesis, as compared to that seen in RKO-LFD mice. These results support the hypothesis that RAGE may contribute to altered energy expenditure and provide a protective effect against DIO by *Ager* deletion. Thus, blocking the RAGE signal transduction axis can be a potential strategy for the treatment of obesity

Table 2. Correlations between the measurement of *UCP1*-mRNA transcripts and BAT activity

Previous work (Song *et al.* 2014) (*UCP1*-mRNA transcripts)	Present study (SUVR = SUV_{iBAT}/SUV_{muscle})
WT-LFD > ½ RKO-LFD	WT-LFD (4.03) > RKO-LFD (2.1); $P = 0.004$
WT-LFD > WT-HFD	WT-LFD (4.03) > WT-HFD (1.4); $P = 0.004$
WT-HFD ≅ RKO-HFD ≥ RKO-LFD	RKO-LFD (2.1) ≥ RKO-HFD (1.52) ≅ WT-HFD (1.4); $P = 0.3$

(Deane *et al.* 2012; Han *et al.* 2012; Han *et al.* 2014; Han *et al.* 2015).

Acknowledgements

We would like to acknowledge the support and assistance of Fei Song, who was a member of the team in Dr. Schmidt's Lab. We also would like to thank the support and assistance of our collaborator, Andrew Gifford, from METIS Labs, NY. The work is supported by The Center for Advanced Imaging Innovation and Research (CAI^2R, *www.cai2r.net*) at New York University School of Medicine is supported by NIH/NIBIB grant number P41 EB017183.

References

Azhdarinia A, Daquinag AC, Tseng C, Ghosh SC, Ghosh P, Amaya-Manzanares F, Sevick-Muraca E and Kolonin MG 2013 A peptide probe for targeted brown adipose tissue imaging. *Nat. Commun.* **4** doi: ARTN 2472 *https://doi.org/10.1038/ncomms3472*

Bao JM, He MY, Liu YW, Lu YJ, Hong YQ, Luo HH, Ren ZL, Zhao SC and Jiang Y 2015 AGE/RAGE/Akt pathway contributes to prostate cancer cell proliferation by promoting Rb phosphorylation and degradation. *Am. J. Cancer. Res.* **5** 1741–1750

Bartelt A and Heeren J 2014 Adipose tissue browning and metabolic health. *Nat. Rev. Endocrinol.* **10** 24–36

Borga M, Virtanen KA, Romu T, Leinhard OD, Persson A, Nuutila P and Enerback S 2014 Brown adipose tissue in humans: Detection and functional analysis using PET (positron emission tomography), MRI (magnetic resonance imaging), and DECT (dual energy computed tomography). *Methods Adipose Tissue Biol., Pt A* **537** 141–159

Cairo M, Villarroya J, Cereijo R, Campderros L, Giralt M and Villarroya F 2016 Thermogenic activation represses autophagy in brown adipose tissue. *Int. J. Obes.* **40** 1591–1599

Cao Q, Hersl J, La H, Smith M, Jenkins J, Goloubeva O, Dilsizian V, Tkaczuk K, Chen WG and Jones L 2014 A pilot study of FDG PET/CT detects a link between brown adipose tissue and breast cancer. *BMC.Cancer.* **14** doi: Artn 12610.1186/1471-2407-14-126

Chavakis T, Bierhaus A and Nawroth PP 2004 RAGE (receptor for advanced glycation end products): A central player in the inflammatory response. *Microbes Infect.* **6** 1219–1225

Cypess AM and Kahn CR 2010 The role and importance of brown adipose tissue in energy homeostasis. *Curr. Opin. Pediatr.* **22** 478–484

Deane R, Singh I, Sagare AP, Bell RD, Ross NT, LaRue B, Love R, Perry S, Paquette N, Deane RJ, Thiyagarajan M, Zarcone T, Fritz G, Friedman AE, Miller BL and Zlokovic BV 2012 A multimodal RAGE-specific inhibitor reduces amyloid beta-mediated brain disorder in a mouse model of Alzheimer disease. *J. Clin. Invest.* **122** 1377–1392

de Jong JMA, Larsson O, Cannon B and Nedergaard J 2015 A stringent validation of mouse adipose tissue identity markers. *Am. J. Physiol.-Endocrinol. Metab.* **308** E1085–E1105

Ding YS 2016 Assessing brown adipose tissue in humans. *Heart Metab.* **69** 15–20

Fromme T and Klingenspor M 2011 Uncoupling protein 1 expression and high-fat diets. *Am. J. Physiol.-Regul. Integr. Comp. Physiol.* **300** R1–R8

Gifford A, Towse TF, Walker RC, Avison MJ and Welch EB 2016 Characterizing active and inactive brown adipose tissue in adult humans using PET-CT and MR imaging. *Am. J. Physiol.-Endocrinol. Metab.* **311** E95–E104

Han YT, Choi GI, Son D, Kim NJ, Yun H, Lee S, Chang DJ, Hong HS, Kim H, Ha HJ, Kim YH, Park HJ, Lee J and Suh YG 2012 Ligand-based design, synthesis, and biological evaluation of 2-aminopyrimidines, a novel series of receptor for advanced glycation end products (RAGE) inhibitors. *J. Med. Chem.* **55** 9120–9135

Han YT, Kim K, Choi GI, An H, Son D, Kim H, Ha HJ, Son JH, Chung SJ, Park HJ, Lee J and Suh YG 2014 Pyrazole-5-carboxamides, novel inhibitors of receptor for advanced glycation end products (RAGE). *Eur. J. Med. Chem.* **79** 128–142

Han YT, Kim K, Son D, An H, Kim H, Lee J, Park HJ, Lee J and Suh YG 2015 Fine tuning of 4,6-bisphenyl-2-(3-alkoxyanilino)pyrimidine focusing on the activity-sensitive aminoalkoxy moiety for a therapeutically useful inhibitor of receptor for advanced glycation end products (RAGE). *Bioorg. Med. Chem.* **23** 579–587

Himms-Hagen J 1990 Brown adipose tissue thermogenesis: Interdisciplinary studies. *FASEB J.* **4** 2890–2898

Hull D and Segall MM 1965 Sympathetic nervous control of brown adipose tissue and heat production in new-born rabbit. *J. Physiol.-London* **181** 458

Hwang JJ, Yeckel CW, Gallezot JD, Belfort-De Aguiar R, Ersahin D, Gao H, Kapinos M, Nabulsi N, Huang YY, Cheng D, Carson RE, Sherwin R and Ding YS 2015 Imaging human brown adipose tissue under room temperature conditions with C-11-MRB, a selective norepinephrine transporter PET ligand. *Metab., Clin. Exp.* **64** 747–755

Innis RB, Cunningham VJ, Delforge J, Fujita M, Giedde A, Gunn RN, Holden J, Houle S, *et al.* 2007 Consensus nomenclature for *in vivo* imaging of reversibly binding radioligands. *J. Cereb. Blood. Flow. Metab.* **27** 1533–1539

Ishiguro H, Nakaigawa N, Miyoshi Y, Fujinami K, Kubota Y and Uemura H 2005 Receptor for advanced glycation end products (RAGE) and its ligand, amphoterin are overexpressed and

associated with prostate cancer development. *Prostate* **64** 92–100

Kozak LP 2014 Genetic variation in brown fat activity and body weight regulation in mice: Lessons for human studies. *Biochim. Et Biophys. Acta-Mol. Basis Dis.* **1842** 370–376

Lau P, Tuong ZK, Wang SC, Fitzsimmons RL, Goode JM, Thomas GP, Cowin GJ, Pearen MA, Mardon K, Stow JL and Muscat GEO 2015 Ror alpha deficiency and decreased adiposity are associated with induction of thermogenic gene expression in subcutaneous white adipose and brown adipose tissue. *Am. J. Physiol.-Endocrinol. Metab.* **308** E159–E171

Lim S, Honek J, Xue Y, Seki T, Cao ZQ, Andersson P, Yang XJ, Hosaka K and Cao YH 2012 Cold-induced activation of brown adipose tissue and adipose angiogenesis in mice. *Nat. Protoc.* **7** 606–615

Lin SF, Fan XN, Yeckel CW, Weinzimmer D, Mulnix T, Gallezot JD, Carson RE, Sherwin RS and Ding YS 2012 Ex vivo and in vivo evaluation of the norepinephrine transporter ligand [C-11]MRB for brown adipose tissue imaging. *Nucl. Med. Biol.* **39** 1081–1086

Mirbolooki MR, Constantinescu CC, Pan ML and Mukherjee J 2011 Quantitative assessment of brown adipose tissue metabolic activity and volume using F-18-FDG PET/CT and beta 3-adrenergic receptor activation. *EJNMMI. Res.* **1**. doi: Artn 3010.1186/2191-219x-1-30

Nedergaard J and Cannon B 2013 UCP1 mRNA does not produce heat. *Biochim. Biophys. Acta* **1831** 943–949

Nirengi S, Yoneshiro T, Sugie H, Saito M and Hamaoka T 2015 Human brown adipose tissue assessed by simple, noninvasive near-infrared time-resolved spectroscopy. *Obesity* **23** 973–980

Nirengi S, Homma T, Inoue N, Sato H, Yoneshiro T, Matsushita M, Kameya T, Sugie H, Tsuzaki K, Saito M, Sakane N, Kurosawa Y and Hamaoka T 2016 Assessment of human brown adipose tissue density during daily ingestion of thermogenic capsinoids using near-infrared time-resolved spectroscopy. *J. Biomed. Opt.* **21**. doi: Artn 09130510.1117/1.Jbo.21.9.091305

Song F, del Pozo CH, Rosario R, Zou YS, Ananthakrishnan R, Xu XY, Patel PR, Benoit VM, Yan SF, Li HL, Friedman RA, Kim JK, Ramasamy R, Ferrante AW and Schmidt AM 2014 RAGE regulates the metabolic and inflammatory response to high-fat feeding in mice. *Diabetes* **63** 1948–1965

Tatsumi M, Engles JM, Ishimori T, Nicely OB, Cohade C and Wahl RL 2004 Intense F-18-FDG uptake in brown fat can be reduced pharmacologically. *J. Nucl. Med.* **45** 1189–1193

Thoonen R, Hindle AG and Scherrer-Crosbie M 2016 Brown adipose tissue: The heat is on the heart. *Am. J. Physiol.-Heart Circ. Physiol.* **310** H1592–H1605

Virtanena KA and Nuutila P 2010 Functional imaging of brown adipose tissue. *Heart Metab.* **48** 15–17

Walden TB, Hansen IR, Timmons JA, Cannon B and Nedergaard J 2012 Recruited vs. Nonrecruited molecular signatures of brown, brite, and white adipose tissues. *Am. J. Physiol.-Endocrinol. Metab.* **302** E19–E31

Wang XK, Minze LJ and Shi ZZ 2012 Functional imaging of brown fat in mice with F-18-FDG micro-PET/CT. *Jove-J. Visualized Exp*. doi: UNSP e406010.3791/4060

Zhuang HM, Cortes-Blanco A, Pourdehnad M, Adam LE, Yamamoto AJ, Martinez-Lazaro R, Lee JH, Loman JC, Rossman MD and Alavi A 2001 Do high glucose levels have differential effect on FDG uptake in inflammatory and malignant disorders? *Nucl. Med. Commun.* **22** 1123–1128

Correponding editor: BJ Rao.